The 15 March 2007 explosive crisis at Stromboli volcano, Italy: Assessing physical parameters through a multidisciplinary approach

M. Pistolesi,[1] D. Delle Donne,[2] L. Pioli,[3] M. Rosi,[1] and M. Ripepe[2]

Received 16 May 2011; revised 4 October 2011; accepted 8 October 2011; published 21 December 2011.

[1] Basaltic volcanoes are dominated by lava emission and mild explosive activity. Nevertheless, many basaltic systems exhibit, from time to time, poorly documented and little-understood violent explosions. A short-lived, multiblast explosive crisis (paroxysmal explosion) occurred on 15 March 2007 during an effusive eruptive crisis at Stromboli (Italy). The explosive crisis, which started at 20:38:14 UT, had a total duration of ~5 min. The combined use of multiparametric data collected by the permanent instrumental networks (seismic, acoustic, and thermal records) and a field survey carried out immediately after the event enabled us to constrain the eruptive dynamics and quantify physical parameters. The eruption consisted of three major pulses: In the first, lithic blocks and ash were ejected at speeds of 100–155 m/s and 130–210 m/s, respectively. The high solid load of the eruptive jet resulted in the partial collapse of the column with the formation of a small-volume pyroclastic density current. The second, 12 s long pulse emitted 2.2–2.7 $\times$ 10^7 kg of tephra (mass discharge rate = 1.9–2.3 $\times$ 10^6 kg/s), forming a 3 km high convective plume, dispersing tephra up to the west coast, and a dilute density current with limited dispersal downslope of the craters. A final, 30 s long phase formed a scoria flow with a volume of 1.5–1.7 $\times$ 10^4 m^3 (mass discharge rate = 5.9–6.7 $\times$ 10^5 kg/s), a total runout of ~200 m, and a velocity of 45 m/s. The total gas volume involved in the explosion was 1.3–1.9 $\times$ 10^4 m^3 with an initial overpressure of 7.9 $\pm$ 0.4 MPa. We compared the 15 March 2007 event with historical paroxysms, in particular with that of 5 April 2003, which was remarkably similar.

Citation: Pistolesi, M., D. Delle Donne, L. Pioli, M. Rosi, and M. Ripepe (2011), The 15 March 2007 explosive crisis at Stromboli volcano, Italy: Assessing physical parameters through a multidisciplinary approach, *J. Geophys. Res.*, *116*, B12206, doi:10.1029/2011JB008527.

1. Introduction

[2] Stromboli is an open-conduit volcano characterized since the Middle Ages by persistent eruptive activity [*Rosi et al.*, 2000]. Usual activity consists of Strombolian explosions from multiple vents and continuous degassing from the summit craters that are aligned along a main direction of diking identified in the edifice striking northeast-southwest [*Tibaldi et al.*, 2003]. The mild explosive activity attracts several thousand tourists each year, who climb the volcano and spend about 1 h on the summit area to watch the explosions from a distance as close as 300 m. Lava flows from lateral vents are confined inside the Sciara del Fuoco, a depression formed by several gravitational collapses [*Tibaldi et al.*, 2003] (Figures 1 and 2a) and often reach the coast, forming short-lived lava-delta-building events (e.g., in 1985, 1993, 2002, 2007 eruptions) [*De Fino et al.*, 1988; *Falsaperla and Spampinato*, 2003; *Bonaccorso et al.*, 2003]. A few times a year, larger explosions (the major explosions are listed by *Barberi et al.* [1993]) disperse ejecta up to a few hundreds of meters away from the vents. More rarely, every few decades, multiblast powerful explosions of a few minutes duration (paroxysms) occur, dispersing pyroclasts up to a few kilometers from the vents [*Barberi et al.*, 1993]. Paroxysms typically consist of a cluster of blasts ejecting meter-sized scoria bombs and blocks up to 2 km from the craters [*Rittmann*, 1931; *Rosi et al.*, 2006] and lapilli and ash up to several kilometers in the atmosphere. Pyroclastic flows have also been reported during paroxysms, occasionally causing injuries and casualties (e.g. 1930 eruption) [*Rittmann*, 1931]. The peculiar feature of Stromboli is its persistent activity and the general steady state conditions of its plumbing system, whose characteristics have remained constant since the Middle Ages [*Rosi et al.*, 2000]. The system is fed by two magma types, differing chiefly in crystal and volatile contents. The current normal activity is fed by the shallow, nearly degassed, and high-porphiricity (HP) magma residing in the volcanic conduit [*Landi et al.*,

[1]Dipartimento di Scienze della Terra, Università di Pisa, Pisa, Italy.
[2]Dipartimento di Scienze della Terra, Università di Firenze, Florence, Italy.
[3]Section des Sciences de la Terre et de l'Environnement, Université de Genève, Geneva, Switzerland.

0148-0227/11/2011JB008527

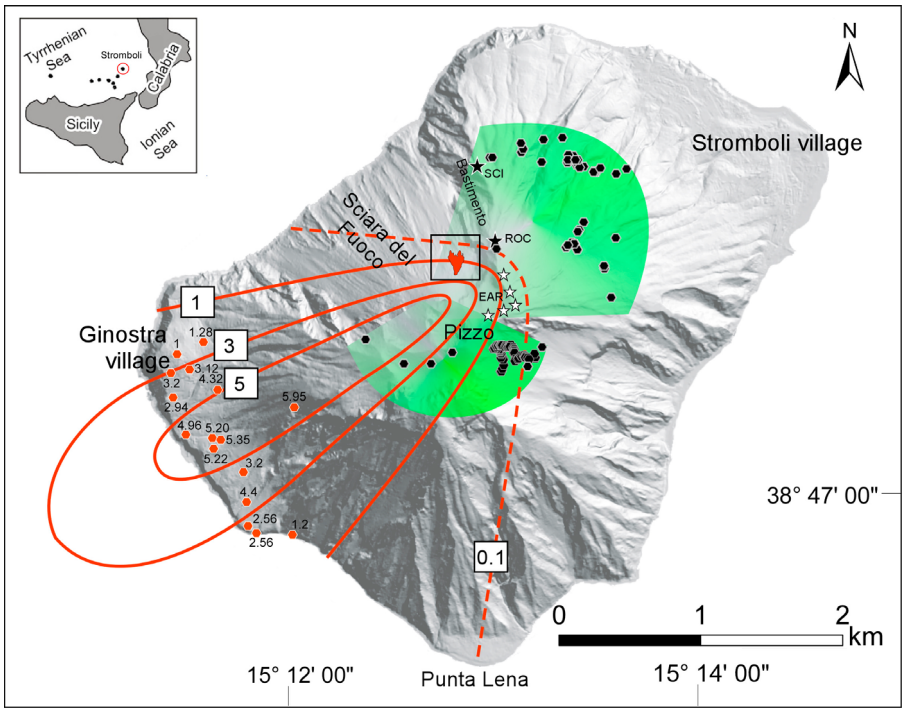

Figure 1. Hillshade map of Stromboli Island. Red curves indicate mass loading per unit area of the 15 March paroxysm; measuring sites are also indicated by red circles (all values expressed in kg/m^2). Black hexagons enclosed in the green shadow area are ballistic blocks mapped in the field. The black box shows the pyroclastic flow deposit emplaced on the lava flow field. The geophysical stations ROC and SCI are indicated with the black star; white stars indicate the EAR station array.

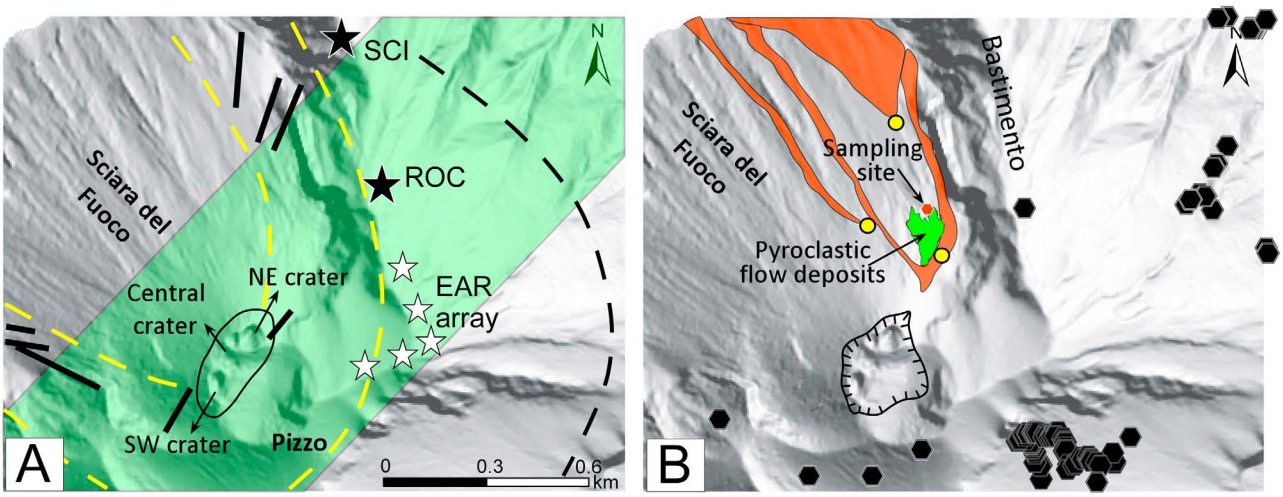

Figure 2. Detailed maps of the crater area (scale bar is the same). (a) The geophysical stations ROC and SCI are indicated with the black star; white stars indicate the EAR station array. The active crater area is indicated by the thin black line. Sector collapse scarps and caldera rims are indicated by yellow and black hatched lines, respectively. The main NE-trending weakness zone (green area) and the proximal dykes (thick black lines) are also reported according to *Tibaldi et al.* [2003]. (b) The pyroclastic flow deposits (green area) and the sampling site (red circle) are indicated. Black hexagons are ballistic blocks mapped in the proximal area. Lava flows (red areas) and lateral vents (yellow circles) alternatively active during the 2007 crisis are also reported. The black hatched line indicates the surface cracks bordering the limit of the summit collapsed area between 3 and 9 March 2007.

2006], which continuously evolves through crystallization (olivine + clinopyroxene + plagioclase). A deep-seated, gas-rich, low-porphiricity (LP) magma reservoir contributes to the renewal of the crystal-rich magma body through decompression and water exsolution induced by H_2O loss, thus continuously refilling the shallow part of the volcano and partially mingling with the crystal-rich body [*Métrich et al.*, 2001; *Francalanci et al.*, 2005]. During paroxysmal eruptions, the deep-seated LP magma can rise in equilibrium with its gas phase (under prevalently closed-system conditions) from a storage zone lying at 7–10 km depth, producing highly vesicular fragments called "golden pumice" [*Bertagnini et al.*, 1999; *Francalanci et al.*, 1999, 2005; *Métrich et al.*, 2001], in addition to crystal-rich scoriae, with virtually the same composition, but with low-crystal and high-volatile contents.

[3] Various hypotheses have been put forward on the structure and behavior of the magma storage between the surface and 10 km depth [*Francalanci et al.*, 2005; *Métrich et al.*, 2001, 2010; *Pompilio and Coltelli*, 1997]. All the models consider the presence at a shallow level of the crystal-rich, high-density (2700 kg/m^3), and high-viscosity (1–4 $\times$ 10^4 Pa s) HP magma that overlies at some unknown depth the crystal-poor, low-density (2500 kg/m^3), and low-viscosity (15–20 Pa s) LP magma [*Métrich et al.*, 2001]. The presence of the denser magma at a shallow level can induce overturns, promoting mechanical mixing between the two magmas and also the formation of highly vesicular blobs that eventually accelerate as they rise (paroxysmal events).

[4] The last two main eruptive crises of the volcano of 2002–2003 and 2007 occurred during the winter, which is the low-tourist season, and thus did not cause any fatalities. Both eruptions started with the emission of lava from lateral fractures, concurrent with the shutoff of the Strombolian activity from the summit craters and the onset of gravitational instabilities in the Sciara del Fuoco, eventually culminating in slope failures (which generated tsunamis in 2003). Paroxysmal explosions also occurred during both effusive crises. Although eruption parameters (ballistic fallout, the duration of eruptive pulses, erupted volume, and the peak mass discharge rate) have been initially quantified for the 5 April 2003 paroxysm [*Calvari et al.*, 2006; *Rosi et al.*, 2006; *Pistolesi et al.*, 2008; *Ripepe and Harris*, 2008], no similar work has been done for the 2007 paroxysm.

[5] We analyze here in detail the dynamics of the 15 March 2007 paroxysm using a multidisciplinary approach that combines field studies of the deposits integrated with a large number of geophysical parameters recorded by the geophysical network of the University of Florence. We also compare the 2003 and 2007 events with other historical paroxysms and discuss the differences in the eruptive parameters of the two events and their possible causes.

2. Chronology of the 2007 Eruptive Crisis

[6] This crisis started on 27 February 2007 and was preceded by 13 days of anomalous high-intensity explosive activity [*Ripepe et al.*, 2009]. A few hours before the onset of the crisis, degassing at the summit craters ceased [*Ripepe et al.*, 2009]. At the same time, the volcano showed significant deformation of the summit cones inducing an increase in the frequency of landslides in the Sciara del Fuoco [*Casagli et al.*, 2009; *Marchetti et al.*, 2009].

[7] The eruptive crisis started with the formation of a fast-moving, 30 m wide, lava flow fed by a new vent that opened at 650 m above sea level (asl) on the flank of the NE crater [*Marchetti et al.*, 2009] (Figure 2b). Emission of lava was accompanied by the complete cessation of the Strombolian activity at the summit craters, located at 750 m asl. During the first hours of the eruption, significant slope movements within the Sciara del Fuoco started, eventually culminating in a landslide and the opening of a second effusive vent at 400 m asl. After the lateral effusive onset, the summit crater terrace was affected by extensional movements and the formation of concentric extension fractures (3–4 March), producing the progressive inward collapse of the summit area that was likely due to the drop of magma level in the main conduit. The collapse of the crater terrace accelerated between 7 and 9 March (Figure 2b) when a large sector of its southern rim gradually slid into the crater, producing a thick pile of debris on the crater floor [*Barberi et al.*, 2009; *Calvari et al.*, 2010]. The volume of collapsed material was estimated at $\sim$1–2 $\times$ 10^6 m^3 [*Marsella et al.*, 2009; *Neri and Lanzafame*, 2009]. An increase in CO_2 and SO_2 emissions occurred between 9 and 15 March, with the CO_2/SO_2 ratio suggesting degassing of a deep magmatic source [*Aiuppa et al.*, 2009; *Burton et al.*, 2009].

[8] On 15 March 2007, while the lava output from the 400 m asl vent was still active, a paroxysmal explosion occurred from the summit vents, producing an eruptive ash column accompanied by lightning. The explosion was preceded by an increase in the effusion rate from the 400 m asl vent starting 9 min before the initial blast [*Ripepe et al.*, 2009]. Tilt and strain anomalies started 6–8 min before the onset of the explosion [*Martini et al.*, 2007; *Ripepe et al.*, 2009]. The fallout of incandescent blocks triggered wildfires, whereas a shower of ash and lapilli blanketed the village of Ginostra (Figure 1). A 200 m long and 120 m wide debris deposit accumulated on the lava flow field, north of the summit craters (Figure 2b). The explosion caused a further widening and deepening of the craters with the removal of a large portion of the southern rim of the crater terrace. In the weeks after the climactic explosion, mild ash emissions resumed at the summit vents and the effusive activity started waning. The gradual decline of the effusion rate resulted in a reduction of flow runout to the complete cessation of the effusive activity on 2 April [*Barberi et al.*, 2009; *Calvari et al.*, 2010].

3. Data Collection

[9] Geophysical data were collected from the integrated monitoring network deployed by the Department of Earth Sciences of the University of Firenze (Figures 1 and 2a). It consists of four broadband seismic stations equipped with calibrated pressure transducers (data from two stations of the network, named ROC and SCI, are used in this work), one five-element infrasonic array (EAR), and one FLIR-A20 thermocamera with a 34° $\times$ 25° optical lens (9.2 mm) and image acquisition at 2 Hz, located at the ROC site, and one Miricle infrared camera with image acquisition at 1 Hz, located at the SCI site. The two cameras are located at 450 and 1000 m from the craters, respectively (Figures 1 and 2a).

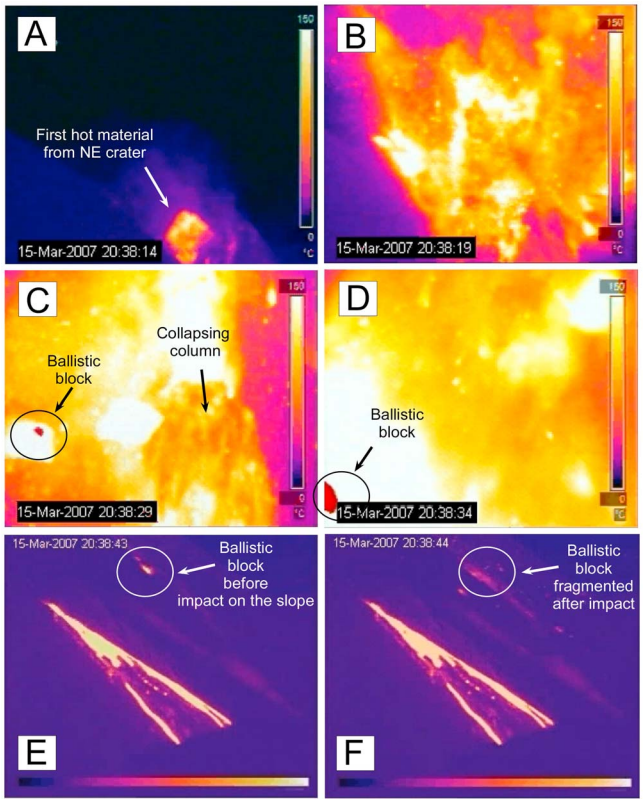

Figure 3. Thermal camera frames of the paroxysm; (a–d) from the ROC station thermal camera and (e, f) from the SCI station (400 m asl). Note big ballistic blocks in Figures 3c and 3d spotted by black circles flying toward the ROC station. From the SCI camera a block is visible to land (Figure 3e) and fragment upon impact (Figure 3f) on the Sciara del Fuoco, close to the active lava flows. The SCI thermal camera was not calibrated for thermal radiance.

The ROC camera was colocated with an infrared thermometer pointing to the NE side of the crater terrace. The thermometer has a maximum thermal resolution of 0.1°C and an uncooled microbolometer sensor with 7.5–13 μm spectral interval of analysis. GPS timing allows the synchronization of all the remote stations of the network.

[10] Field surveys on fallout deposits were carried out two days after the event on the distal area (Ginostra village) and in the following days on the NE slope of the volcano, where several ballistic blocks were measured and mapped (Figure 1). During fieldwork, measurements of mass loading per unit area and sampling of the tephra were carried out. Two 1 m deep trenches were also dug in the pyroclastic flow deposit emplaced during the event on the lava flow field at ~700 m asl in July 2007 and September 2008 for stratigraphic observations and deposit sampling.

[11] Field studies of deposits were complemented with an analysis of the physical properties of juvenile material. Bulk densities of juvenile clasts were measured on 120 individual pumice fragments of uniform grain size (2–4 cm) collected at distal sites (Ginostra village). After cleaning and drying, clasts were sealed with cellulose acetate and bulk density determined by the immersion technique.

[12] Grain-size measurements were carried out with standard laboratory dry sieving at half-φ intervals (where $\varphi = -\log_2 D$, in which D is the particle diameter in millimeters) and, for breccia deposits, sieving both in the field and in the lab. Grain-size parameters were calculated after the works by *Inman* [1952] and *Folk and Ward* [1957].

4. Thermal Camera Records of the Paroxysmal Phase

[13] The paroxysmal explosion was recorded by the thermal cameras installed around the crater area. The ROC thermal camera recorded some glowing at 20:38:09 UT at the base of the NE crater. The 15 March 2007 explosion started at 20:38:14 UT (Figure 3a) when the camera detected a fast-rising jet of hot material from the NE sector of the crater terrace. A V-shaped, NW-SE-oriented jet rose with a vertical angle of about 60° and consisted of a high-temperature mixture of gas, ash and bombs. After ~5 s, the camera recorded an eruptive jet of individual ballistic blocks (Figure 3b), hot enough to saturate the thermal camera (>150°C) and striking the ground ~15 s after the eruption onset (Figures 3c and 3d). At 20:38:24 UT, the central part of the jet collapsed toward the NE (Figure 3c). Images taken by the Instituto Nazionale de Geofisica e Vulcanologia (INGV) thermal camera from a lower cliff NE of the crater showed that the collapsed cloud was partly channeled toward the lava flow field [*Calvari et al.*, 2010]. The camera field of view was then partially obscured by the hot material, but a second vertical jet lasting ~12 s was observed between 20:38:36 UT and 20:38:48 UT. The fallout of ballistic blocks was recorded until 20:38:44 UT (30 s after eruption onset) by the SCI thermal camera at 400 m asl (Figures 3e and 3f), although a minor continuous fallout of hot material near the ROC camera was recorded until 20:39:16 UT.

[14] After this time, eruptive activity waned and the camera field of view began to clear. No explosions were recorded by the thermal camera and the seismic stations until 20:41:33 UT, when a new hot cloud was observed to form above the vents and then spread laterally from the NE crater toward the Sciara del Fuoco, without the formation of a vertical eruptive jet. A final ash emission lasting a few seconds was recorded at 20:42:50 UT from the northern sector of the NE crater.

[15] The eruptive activity, as recorded by the thermal cameras, can thus be divided into three pulses:

[16] 1. Pulse I (20:38:14–20:38:36 UT): formation of a V-shaped jet coupled with the launch of bombs and blocks and followed by the collapse of the central part of the eruptive column onto the lava flow field.

[17] 2. Pulse II (20:38:36–~20:39:16 UT): formation of a second vertical gas and ash jet lasting ~12 s accompanied by the contemporaneous fallout of ballistic blocks.

[18] 3. Pulse III (20:41:33–20:43:00 UT): "boiling-over" activity of eruptive material from the NE crater, spilling over through the NE crater notch and feeding a dense, hot pyroclastic flow.

5. Characteristics of Pyroclastic Deposits

[19] Field observations of the eruptive products were conducted in several surveys carried out between 2007 and

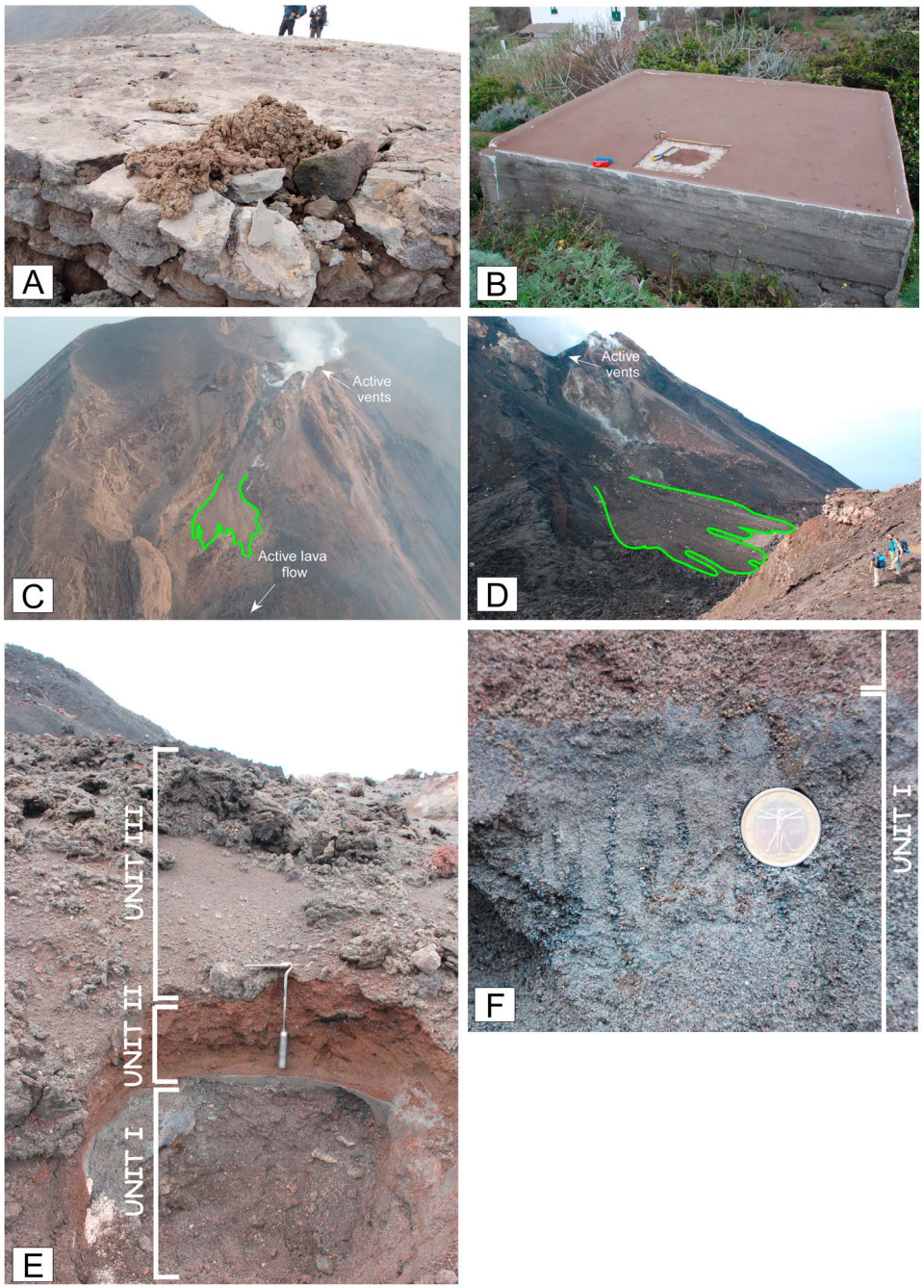

Figure 4. (a) Spatter bomb on the helipad, along the trail between ROC and Pizzo; (b) ash sampling and measurements of mass loading per unit area in Ginostra village; (c) northern sector view; note the scoria flow deposit on the lava field (green line) and the active lava flows; (d) the scoria flow deposit (green line) as seen from the Bastimento ridge; (e) stratigraphic section of the pyroclastic flow deposits overlaying the lavas; (f) close-up of the degassing pipes at the top of unit I.

2008. The fallout deposit, in particular, was examined in the days immediately after the explosion and before any rainfall.

[20] The tephra deposits consist mainly of (i) fallout of scattered coarse to very coarse pumice clasts in the proximal area (Figure 4a), grading into a fine-grained (lapilli and ash) fallout blanket dispersed to the southwest (Ginostra village, Figures 1 and 4b); (ii) ballistic blocks and bombs deposited around the crater area and on the NE slope of the volcano; and (iii) pyroclastic flow deposits accumulated on the lava field at 700 m asl (Figures 4c and 4d). The overall sequence exhibits excellent consistency with the eruptive pulses recorded by the thermal cameras.

5.1. Ash and Lapilli Fallout Deposit

[21] A continuous fallout blanket (2–3 cm thick, Figure 1) was deposited over a 90° wide arc SW of the crater area. The

deposit consists of scattered, coarse to medium lapilli set in a well-sorted, red, coarse ash matrix ($Md_\varphi = 0.58\varphi$; $\sigma_\varphi = 2.08$). The juvenile component accounts for 38 wt %, whereas the majority of the deposit is composed of oxidized, hydrothermally altered lithic clasts (62 wt %). Pumice clasts show high variability in shape, from rounded to elongated to flattened. The mass per unit area of the deposit was measured at 16 sites in the days between 19 and 23 March 2007, and the ash deposited over 1 m^2 sampling surfaces (Figure 4b) was collected. Ash was mainly collected on the tops of the flat roofs in the village of Ginostra. Isomass curves obtained by linear interpolation of individual data points are presented in Figure 1. Loading per unit area of fallout deposit versus isomass area plot shows a single exponential decay law; consequently, the volume of the fallout deposit was calculated according to the work by *Pyle* [1989], giving a value of 1.7–2 $\times$ 10^4 m^3.

5.2. Ballistic Bombs and Blocks

[22] The thermal camera records indicate that most of the blocks falling over the northeast sector were emitted during pulse I of the eruption. Scattered fallout of 30–40 cm long spatter bombs with an average distribution of 1 block per 4 m^2 occurred around the crater area and toward the southeast of the volcano (Figure 4a).

[23] Angular ballistic blocks that landed on the NE sector were analyzed within a few days after the event, when the lack of alteration made the identification of products unequivocal. During this survey, we collected the size and GPS coordinates of 111 blocks or impact craters (Figure 1). Two main areas were affected by block fallout: the NE sector around the crater area (Figures 5a and 5b) and the area along the trail that crosses the slope at 400 m asl (Figures 5c–5g). All blocks that fell on vegetated areas charred the vegetation (Figure 5d), indicating that they were at a high temperature when they landed.

[24] Equivalent block diameters were between 0.3 and 2 m, with ballistic distances from 400 to 1300 m from the active vents. Three main categories of lithic blocks were observed: (i) poorly vesiculated, holocrystalline lavas (Figure 5e); (ii) strongly altered agglutinated scoria bombs (Figure 5f); (iii) dm-sized lava and scoria clasts with slight to moderate alteration. Some blocks showed cracks on external surfaces upon impact on the ground.

5.3. Pyroclastic Flow Deposits

[25] Pyroclastic density current deposits accumulated on the lava field at 700 m asl and at a distance of about 380 m north from the NE crater. The deposit sequence was examined and sampled in two 1 m deep trenches dug at the base of a flow lobe in July 2008 (about 370 m from the active vents) (Figures 4e and 4f). The overall sequence is composed of both dilute current deposits (surge deposits) with limited thickness and coarse-grained, dense pyroclastic flow deposits that formed distinct, sharply edged, and highly visible units dotted with large blocks (Figures 1, 4c, and 4d). The substratum of the pyroclastic sequence (Figure 4e) is the lava emplaced a couple of weeks before (27 February 2007); the lava is overlaid by a thin layer of white ash (thickness ~2 mm), probably deposited between 27 February and 15 March 2007.

[26] The pyroclastic flow sequence is divided into three main units (Figure 6). Unit I is a 50–60 cm thick, normally graded, dark gray colored, loose breccia bed. The deposit bears blocks up to 20–25 cm in diameter set within an ash matrix, and shows prominent normal grading in its upper part. Grain-size parameters confirm the moderate sorting (σ_φ from 1.9 to 1.6) and the normal grading (Md_φ from 0.9 to 2φ upward). The deposit consists exclusively of hydrothermally altered scoria and lava with no fresh juvenile material. Well-developed, thin degassing pipes occur within the upper third of unit I; the pipes were directly connected to a millimeter-thick, discontinuous, fine-grained ash layer on top of the breccia, probably deposited by the ashy gas (Figure 4f). Degassing pipes formed probably within seconds immediately after unit I came to rest as they were sealed by the overlying unit II. A 5 cm thick layer of dark gray ash with the same color and composition of unit I occurs between the top of the pipes and unit II. This bed could have either been deposited by the delayed arrival of the same density current after it had been deflected by the Bastimento ridge back to the lava flow field or produced by another smaller burst.

[27] Unit II consists of a normally graded, 30 cm thick layer of red ash bearing scattered lapilli of golden pumice and black scoria (Figures 7a and 7c). The juvenile/lithic weight ratio is ~0.6; thus it is similar to the one found for the distal fallout deposit collected in Ginostra village along the dispersal axis (juvenile golden pumice clasts 12 wt %, black scoria clasts 26 wt %, and lithic clasts 62 wt %). Secondary crystals of gypsum and sulfur fill open pores of the deposit, with concentrations decreasing from bottom to top; the preserved euhedral crystal shapes indicate that both minerals crystallized in situ at high temperatures from gas percolating through the deposit produced by the degassing lava or trapped during the emplacement of the breccia. It was not possible to precisely map units I and II: we estimated a collective volume for the two units to be of the order of 10^4–10^5 m^3; however, these were not computed in further calculations as these deposits are made only by lithic, altered material.

[28] Unit III is a lithic-rich, coarse-grained lapilli and scoria deposit whose boundary is limited by sharp edges. Grain-size parameters, obtained by processing about 135 kg of dry deposit, confirmed a coarse grain size ($Md_\varphi = -6.8\varphi$) and poor sorting ($\sigma_\varphi = 3.9$). The juvenile component consists of equidimensional to flattened or twisted bombs of golden pumice with a maximum diameter of 40 cm, many with a textural roughness and ribs on the external surface. The lithic component (30–40 vol %) consists of oxidized clasts, black unaltered scoria clasts, and fragments variably affected by fumarolic alteration. The deposit is dispersed over an area of 1.0 $\times$ 10^4 m^2 and, assuming an average thickness of 1.5 m, has an estimated volume of 1.5–1.7 $\times$ 10^4 m^3. Component analysis indicates that the golden pumice was much more abundant in unit III than in unit II.

[29] In our interpretation, on the basis of thermal camera records and field characteristics, we consider unit I as related to a dilute pyroclastic current that reached the lava field after the column collapse of pulse I, sealed by a second surge unit (unit II) fed by the second jet of the eruptive sequence (pulse II), which also led to the formation of a convective plume and to the deposition of the windblown fallout over

Figure 5. (a) Ballistic block (1.4 m in diameter) fallen close to the ROC station, on the Bastimento ridge at 740 m asl (the station is in the background); (b) shelter on the Bastimento damaged by the block fallout; (c) impact crater on the northeastern slope, with the Stromboli village in the background; (d) vegetation on the northeastern slope burnt by ballistic fallout (block visible in the background); (e) unaltered, poorly vesiculated gray lava block fallen on the trail at 400 m asl (lens cap for scale); (f) hydrothermally altered ballistic clast on the northeastern slope; (g) impact crater along the trail on the northeastern slope, at 510 m asl; impact fractures on the ground are visible on the right. Figures 5c and 5g are courtesy of T. Ricci.

Ginostra village. Unit III is related to the emplacement of a coarse-grained, valley-confined, scoria flow deposit formed by the "boiling-over" activity of the NE crater during the final stage of the eruption.

5.4. Physical Characteristics of the Juvenile Material

[30] Density values of the juvenile material range from 260 to 1080 kg/m^3 (average 600 $\pm$ 170 kg/m^3), corresponding to a range of vesicularity of 65 to 95 vol% (mean = 85 vol%; Figure 8), calculated using a measured dense-rock-equivalent (DRE) density of 2850 $\pm$ 40 kg/m^3. Clast vesicularity has a narrow unimodal distribution with a low-density tail, representing about 10% of the clasts (Figure 8). The mingling proportion between the crystal-rich (volatile-poor) component and the crystal-poor (volatile-rich) components (Figure 7b) is considered the main factor controlling the vesicularity of

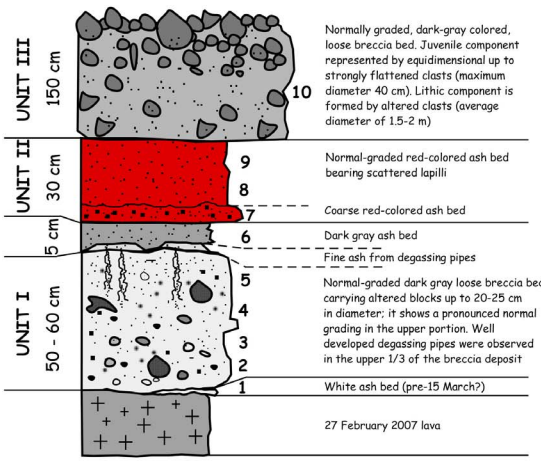

Sample	MdΦ	σΦ	Juvenile (pumice) wt%	Juvenile (scoria) wt%	Lithics wt%
10	-6.5	3.9	80.1	0	19.9
9	2.2	1.3	-	-	-
8	2.1	1.3	14.7	22.4	62.9
7	1.1	1.7	-	-	-
6	3.2	1.1	0	20.9	79.1
5	2.0	1.6	-	-	-
4	0.8	1.9	0	0	100
3	0.9	1.9	0	0	100
2	0.9	1.8	0	0	100
1	3	1.3	-	-	-

Figure 6. Reconstructed stratigraphic section of the 15 March 2007 deposits on the active lava flow field. Description, grain size, and component parameters of units and subunits are also indicated.

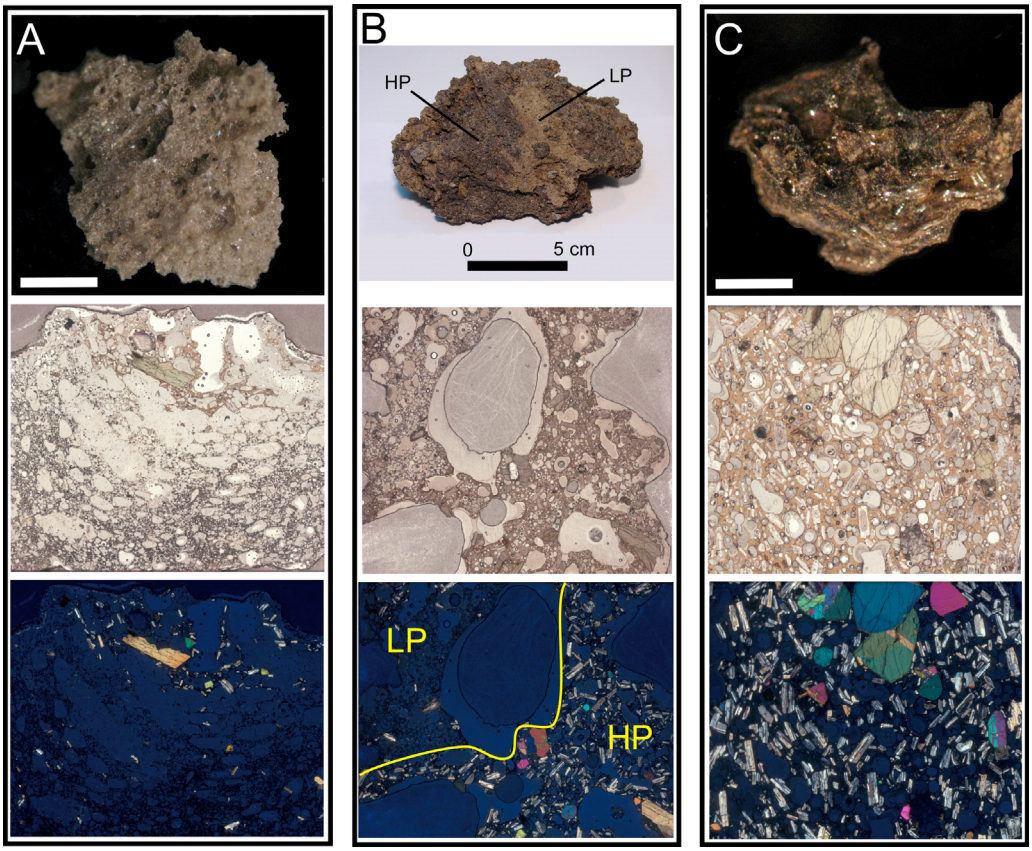

Figure 7. Stromboli tephra clasts. (a) LP ash clast of the 15 March 2007 deposit and its inner part (0.5 × 0.5 cm) in a thin section, both with parallel and crossed nicols. Note the scarcity of crystals and the high vesicularity. (b) HP-LP mingled hand specimen of the 5 April 2003 paroxysm with its inner part (0.5 × 0.5 cm) in a thin section; LP and HP parts are separated by the yellow line and coexist in the same pumice. (c) HP scoriaceous ash clast of the 15 March 2007 paroxysm and its inner part (0.5 × 0.5 cm) in a thin section. Phenocrysts and microphenocrysts (mainly olivine and plagioclase) are much more abundant than in 7a. White scale bars are 0.5 cm.

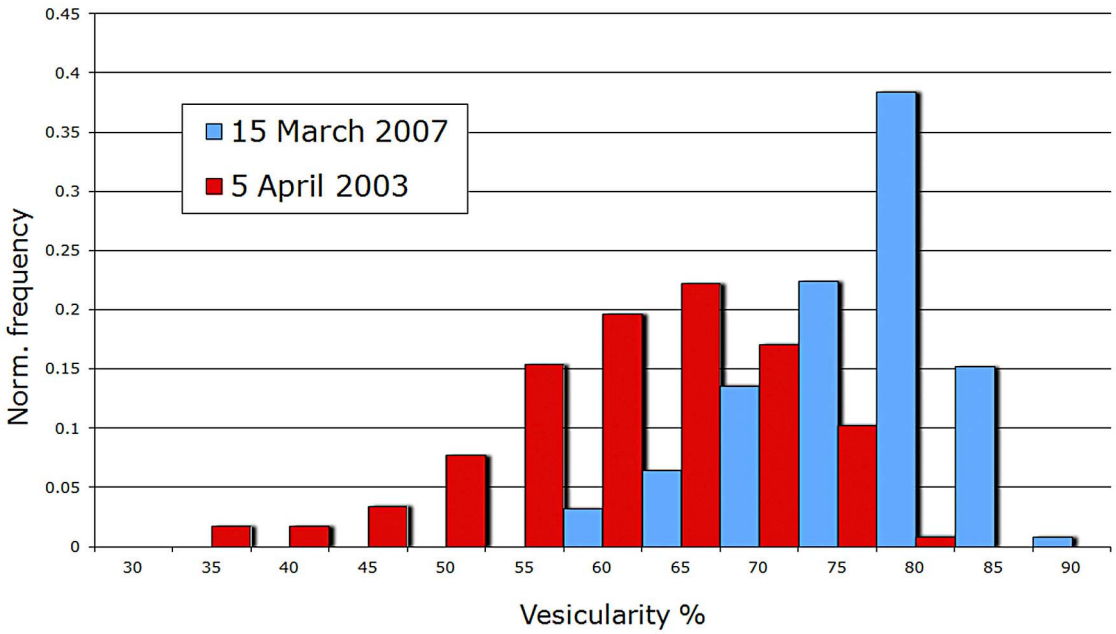

Figure 8. Frequency histogram of vesicularity distribution of 15 March 2007 (blue bars) and 5 April 2003 paroxysms (red bars). 120 specimens, collected in the Ginostra village area (15 March 2007) and along the Punta Lena coast (5 April 2003), were analyzed for each event. 5 April data are from the work by *Pistolesi et al.* [2008].

juvenile material ejected during paroxysmal explosions of Stromboli [*Bertagnini et al.*, 1999; *Francalanci et al.*, 1999, 2005; *Métrich et al.*, 2001]. The very high mean vesicularity and the narrow unimodal distribution of the analyzed clasts (centimeter scale) reflect the relatively scarce amount of crystal-rich (HP) component in the juvenile material of 2007. This suggests that the rise of the LP magma,within the HP magma filling the shallow conduit, was such to minimize the mechanical interaction between the two magmas with an inferred contrasting density and viscosity [*Carrigan*, 1994; *Freundt and Tait*, 1986].

6. Geophysical Data

[31] Synchronized thermal images, seismic, infrasonic, and infrared signals enabled us to track the onset, to detail the evolution and duration of the different eruptive pulses, and to measure and calculate several eruption parameters.

6.1. Thermal Monitoring

[32] The infrared radiometer is located in a direct line of sight with the NE crater, so that the onset of the radiometric transient can be considered the initial time of the injection of volcanic material into the atmosphere (t1, Figure 9e).

[33] The IR thermometer detected the first hot material at 20:38:14 UT; the record shows an abrupt increase during which the integrated temperature within the field of view increased by ~100°C in 1.15 s (point a in Figure 9e).

[34] The thermal record shows two prominent spikes: the first occurred at 20:38:35 UT and is related to relatively cold material already obscuring the thermometer field of view. The second spike occurred at 20:38:37 UT (20 s after the thermal onset), and the cross correlation with the thermal camera indicates that this is related to the passage, within the proximity of the thermometer, of three big incandescent ballistic blocks that landed close to the ROC station (Figures 3c, 3d, and 5a). The first block described a parabola parallel to the camera view angle and is responsible for the second low-amplitude oscillation. The second and third blocks were also observed in the thermal video, and they could be correlated with the two spikes.

6.2. Seismic and Infrasonic Monitoring

[35] Seismic and infrasonic signals related to the eruption recorded at the ROC site are shown in Figures 9c and 9d, respectively. Because of the proximity of the ROC station to the crater area (~450 m), the seismic signal was clipped during most of the event. However, it is still possible to define a gradual increase of tremor amplitude ~75 s before the eruption onset.

[36] The onset of the pressure wave associated with the blast is marked as t2 (Figure 9d), and the difference between the t2 and t1 times is related to the transit time for compressional air waves to propagate 450 m at a speed of 340 m/s (~1.22 s). After t3 (Figure 9c), the seismic signal shows a typical waveform related to a sort of recalibration curve. We interpreted this out-of-leveling as produced by the landing of the $\sim 3.6 \times 10^3$ kg block in the proximity of the recording site. The difference between the T3 and T1 times would correspond to the flight time of the block, thus allowing an estimate of the initial velocity of the block (see section 7.1).

6.3. Linking Field Observations With Geophysical Monitoring

[37] The SCI station, located about 1000 m north of the crater area, recorded the eruptive sequence without a significant clipping of the signal (Figure 10). This has allowed us to compare the timing of the main eruptive pulses (as reconstructed from both thermal cameras; Figure 10a) with

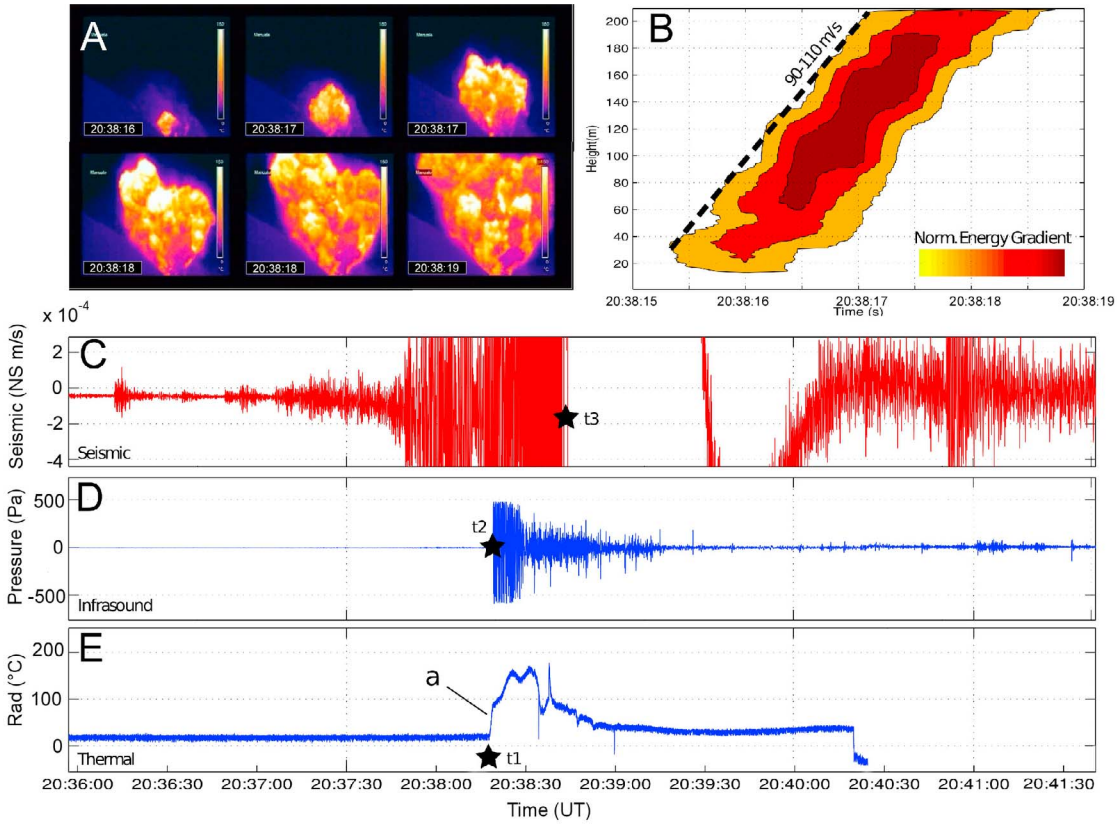

Figure 9. (a) Frames of the eruption onset (pulse I) from the ROC thermal camera, showing the V-shaped, NW-SE oriented jet of high-temperature gas, ash, and bombs between 20:38:16 and 20:38:19 of the 15 March 2007 event. The camera field of view is 320 × 260 m; (b) plot of thermal energy variation along the vertical direction in the time of consecutive images for the six frames in 9a; thermal energy is calculated from temperature using the Stefan-Boltzmann law ($E = \sigma T^4$); the slope of the line corresponds to the ascent velocity of the jet. (c) Seismic, (d) acoustic, and (e) thermal logs of the event from the ROC station. Black stars correspond to t1 (thermal onset), t2 (acoustic onset), and t3 (clip of the seismic signal); "a" corresponds to the abrupt increase recorded by the IR thermometer.

seismic and infrasonic signals recorded at the SCI station (Figures 10b and 10c). Infrasonic array processing using the multichannel semblance method [*Ripepe and Marchetti*, 2002] allows the identification of different phases in the infrasonic record (Figure 10c). Back-azimuth directions (Figure 10d) show coherent infrasound signals mainly coming from the crater area. These events are interpreted as intense degassing at the crater. Two seismic events occurred after the pre-eruptive tremor and are separated by a relatively high tremor phase (Figure 10b).

[38] During pulse I (Figure 10a), both seismic and acoustic signals show an abrupt increase correlated with an increase in frequency. We interpret this increase as a consequence of the column collapse combined with a fast-moving pyroclastic density current moving toward the SCI station. The collapse lasted 10 s, and the interpreted presence of a fast-moving pyroclastic flow generated by the column collapse is supported also by the progressive shift of the infrasonic source (Figure 10d) toward the Sciara del Fuoco.

[39] A second, 12 s long jet (pulse II) formed while both the seismic and infrasonic signals showed a progressive decay (which was likely due to the halt of the pyroclastic flow). A strong degassing phase characterized by high tremor and scarce visibility then followed. During this phase, a second main event is visible both in the seismic and acoustic records (Figures 10b and 10c). Once the crater area had cleared, the thermal camera recorded a low plume at the NE crater and an ash cloud rising from the lava flow field (pulse III). This observation suggests a final boiling-over activity leading to the formation of a dense pyroclastic flow. Although the second seismic event is not associated with any infrasonic location, the similarity of the frequency content with the first signal is consistent with a small-volume pyroclastic flow.

[40] Although most of the seismic energy during pulse III is limited in the 3–7 Hz band, which is typical also for rockfalls and gravity-induced landslides [*Pino et al.*, 2004], the infrasonic signal is characterized by a strong low-frequency component (1 Hz), which is typical for pyroclastic flows [*Ripepe et al.*, 2009].

7. Eruption Parameters for 15 March 2007

7.1. Plume Dynamics

[41] Plume dynamics parameters are derived here following the same procedure used by *Ripepe and Harris* [2008] to analyze the paroxysm of 5 April 2003 at Stromboli.

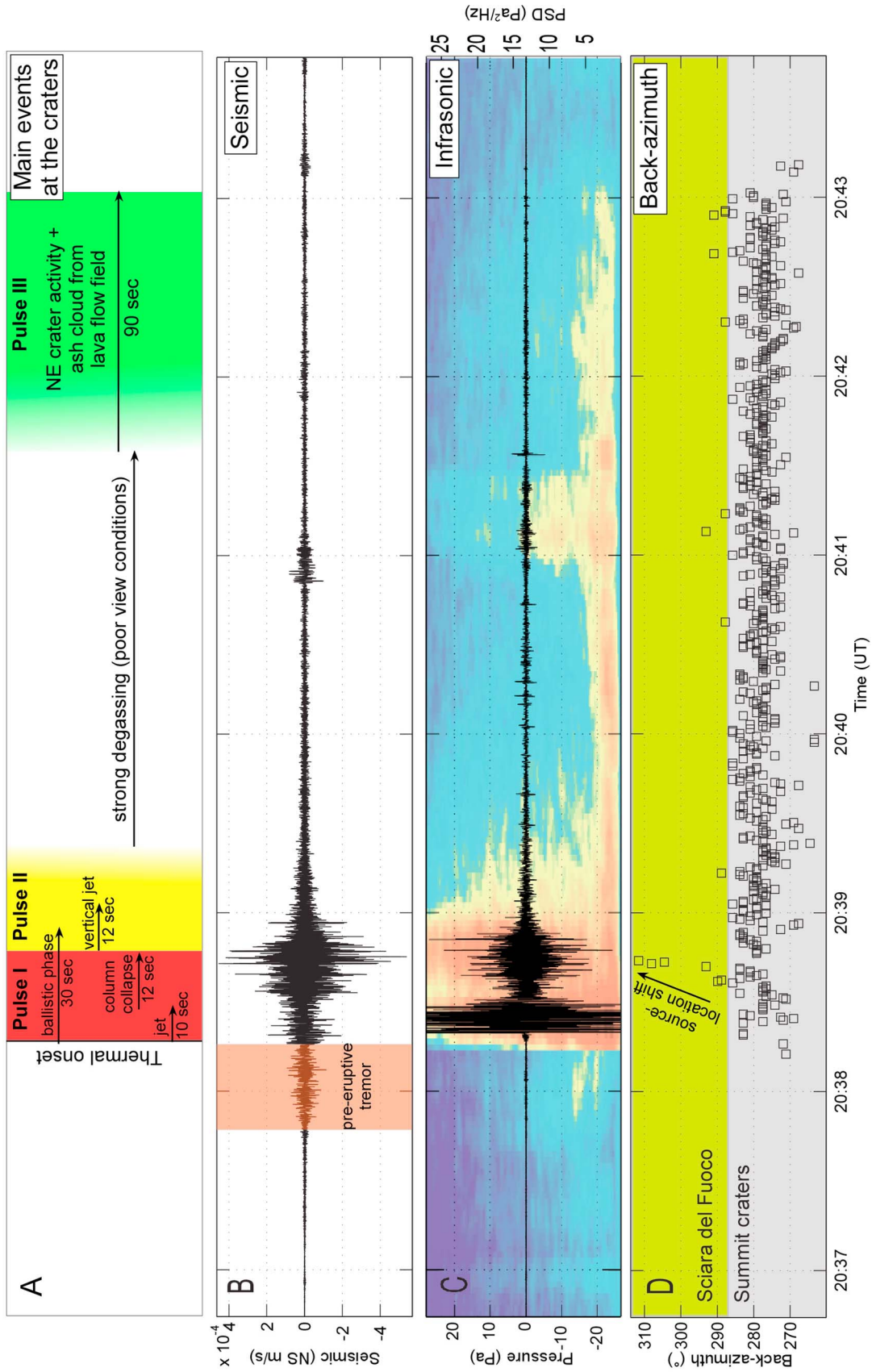

Figure 10. (a) Main events (pulses) occurred at the craters recorded by the thermal cameras at Stromboli on the 15 March 2007; (b) seismic and (c) infrasonic signals, and (d) infrasonic back-azimuth values associated with the explosion recorded at SCI station, located 1000 m away from the craters. Seismic record shows an increase in the seismic tremor (brown bar in Figure 10b) preceding the main blast. The back-azimuth diagram evaluated from infrasonic array EAR (Figure 10d) reveals a shift of the source location compatible with the emplacement of the surge generated by the column collapse of pulse I.

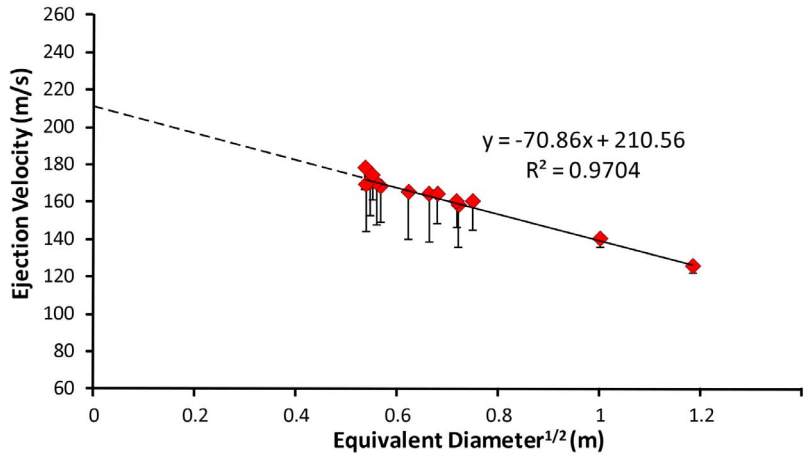

Figure 11. Ballistic block ejection velocities versus square root of block equivalent diameters. The gas velocity is calculated as the theoretical speed of particles with infinitesimal diameter (the intercept of the best fit line along the velocity axis with square root of block equivalent diameters = 0). The first point on the right (v = 126 m/s) represents the block fallen close to the ROC station (Figure 5a). Diamonds represent the maximum calculated velocities, whose values are best fitting to a straight line. The entire range of possible velocities, obtained by combining different launch angles and flight times, is shown as a vertical bar.

[42] As observed from thermal records, pulse I of the event was characterized by the launch of ballistic blocks. Exit velocities of blocks were calculated using two different approaches. First, the seismometer of the ROC station went out of scale when the 3.6×10^3 kg block landed ~10 m from the station (Figure 5a), causing a strong local ground displacement (T3 in Figure 9c). The onset of the off-scale episode in the seismic record provides the flight time of the block (25.5 s), which, in turn, can be converted with the method of *Ripepe and Harris* [2008] by using a block area of 1.5 m^2 and a block density of 2500 kg/m^3, to an ejection velocity of 126 m/s, a launch angle of 75°, and a maximum elevation of 500 m above the vent.

[43] We also used the ballistic equations that control flight time and range for a particle of a given size as a function of drag, e.g., *Eject* [*Mastin*, 2001] to calculate the trajectory of 12 blocks mapped on the NE slope. Blocks ranging from 0.3 to 0.5 in equivalent diameters landed at a distance of 970–1360 m from the vent with Δh between vent and landing points from 270 to 515 m.

[44] The time of flight and the launch angle are unknown (apart from the block that fell close to the ROC station) and are interdependent values. We therefore estimate time of flight and launch angle using thermal images from the SCI and ROC cameras. From the images, we estimate that the flight times can range between 15 and 30 s while the launch angles can range between a minimum of 58° (as observed from the camera) and 90°.

[45] Minimum velocities are calculated using the minimum launch angle of 58°, whereas the maximum velocities are obtained by increasing the launch angle in order to match the maximum flight time recorded (30 s, as observed from the SCI thermal camera). We thus obtain a range of velocity of 100–155 m/s and a maximum launch angle of ~75°. Lower velocities of 100–120 m/s are associated with a launch angle of 58° and a travel time of ~15 s.

[46] Assuming that the blocks reached their terminal velocity within the conduit, the gas-ash cloud velocity (U_{cloud}) is also related to the velocities of the large blocks (U_{ejecta}) by the equation of motion [*Steinberg and Babenko*, 1978]:

$$U_{cloud} = U_{ejecta} + \left[\frac{4g\rho_{ejecta}}{3C_D\rho_{cloud}}\right]\sqrt{D}, \qquad (1)$$

where ρ_{ejecta} is the density of ballistic blocks, ρ_{cloud} is the gas-ash cloud density, and C_D is the drag coefficient. We can thus calculate gas velocity once U_{ejecta} and the diameter of the fragments (D) are known [*Ripepe et al.*, 2001] by assuming that the gas velocity is equal to the velocity of those particles with infinitesimal diameter (Figure 11). From the velocities obtained for the mapped blocks of the NE sector, we calculate a gas-ash cloud velocity of 210 ± 40 m/s.

[47] The gas-ash cloud exit velocity during the first seconds of the explosion can also be evaluated from the thermal images using two independent methods. By measuring the time (~3 s) for hot material to completely fill the camera field of view (240 m), we calculate an exit velocity of 130 m/s (Figure 9a). The second method tracks the vertical propagation of the jet front in consecutive frames from thermal images [*Delle Donne et al.*, 2006; *Marchetti et al.*, 2009] as a function of the thermal energy variation (Figure 9b). Thermal energy E is calculated from the temperature using the Stefan-Boltzmann law ($E = \sigma T^4$), where σ is the Stefan-Boltzmann constant. The linear trend of the thermal energy gradient as a function of height allows us to estimate the average upward plume velocity in the first two seconds of the explosion to be between 90 and 110 m/s.

[48] The discrepancy between the velocities obtained with the thermal image analysis (90–130 m/s) compared with the "ballistic" method (210 ± 40 m/s) could be partially due to the drop of the magmatic column that occurred in the weeks

before the explosion. The first jet of hot material seen by the camera had already traveled (and thus decelerated) for at least ~100 m in the conduit, whereas ballistic calculation is not affected by depth bias once the launch time is set.

[49] From equation (1), we can also evaluate the gas-ash cloud density (ρ_{cloud}) by using the maximum gas velocity (210 ± 40 m/s) calculated from the velocity of the ballistic blocks. We obtain an initial cloud density of 13.5 ± 3 kg/m^3. The calculated gas-ash-cloud density (ρ_{cloud}) can be converted to an overpressure of 7.9 ± 0.4 MPa following the ideal gas law, considering that Stromboli's gas is mainly (>80%) H_2O.

[50] From the Bernoulli modified equation [*Self et al.*, 1979],

$$U_{cloud}^2 = 2\left[\frac{nRT}{m}\ln\left(\frac{P_{cloud}}{P_{atm}}\right) + \frac{1-n}{\rho_{ejecta}}(P_{cloud} - P_{atm})\right], \qquad (2)$$

in which R is the universal gas constant (8.314 J/mol K), m is the molecular gas mass (0.018 kg/mol), T is the absolute gas temperature (1270 K), and P_{cloud} is the overpressure of the gas-ash cloud, we also calculate a gas mass fraction (n) of 0.008 (if the gas is at atmospheric pressure). As the gas mass fraction represents the ratio between the gas mass and total mass of ejecta and ash involved in the explosion, we estimate a total gas mass of 1.9–2.3 × 10^5 kg (with a total mass of 2.5 × 10^7 kg). Using the gas-ash cloud density of 13.5 ± 3 kg/m^3, this converts to a gas volume of 1.3–1.9 × 10^4 m^3.

[51] As the explosion can be considered a transient event, the total amount of heat release and the total mass of erupted material control the plume height [*Parfitt and Wilson*, 2008]:

$$H = 0.042 M_e^{1/4}, \qquad (3)$$

where H is the column height and M_e is the total mass of solids and gas ejected; we obtained a value of 2.9 km that is in good agreement with estimation from satellite images [*Spinetti et al.*, 2007]. Assuming a simplified cylinder shape for the conduit, we finally calculate a vent radius of 4 m using the calculated mass flux, the calculated ejection velocity, and 12 s as the total duration of the main event (pulse II).

7.2. Pyroclastic Flow Kinematics

[52] The occurrence of a pyroclastic flow event was also reported during the 5 April 2003 paroxysm [*Rosi et al.*, 2006]. Here we can make use of the multiparametric monitoring system present on Stromboli and the field survey performed briefly after the paroxysm to characterize the pyroclastic flow kinematics. Besides the field evidence, the occurrence of a moving pyroclastic flow generated by the column collapse is supported by the progressive shift of the infrasonic source (Figure 10d) toward the Sciara del Fuoco.

[53] The change of infrasonic source with time, shifting from 283°N to 311°N with respect to the central microphone of the EAR array, is related to an angular displacement of 28° of the flow toward the northeast. Assuming that the pyroclastic flow has traveled along the maximum topographic gradient, the flow trajectory is obtained by intersecting the back-azimuth directions with the topography. This allows a conversion of the back-azimuth shift of 28° to a runout of 185 m (which is consistent with field observations). Considering that this distance was well covered in 4.15 s, we thus estimate a mean velocity of ~45 m/s, which is in good agreement with previous measurements of pyroclastic flows calculated, for example, at Unzen [*Yamasato*, 1997] and at Soufrière Hills volcanoes [*Ripepe et al.*, 2009] by infrasonic measurements and with numerical simulations [*Hooper and Mattioli*, 2001].

8. Eruption Dynamics

[54] The 15 March 2007 paroxysm lasted for about 5 min and consisted of a series of discrete explosive pulses from the summit vents; the explosive sequence was preceded by the inflation and the seaward sliding of the summit that were likely due to the pressurization within the conduit [*Casagli et al.*, 2009; *Ripepe et al.*, 2009]. The explosion started at 20:38:14 UT when the IR thermometer detected the first impulse of hot material, and it was preceded by an increase in the level of seismic tremor.

[55] The paroxysm consisted of two jets in fairly rapid sequence (pulse I + pulse II), emitting ballistic blocks and forming a 2.9 km high convective column. Both jets culminated with the partial collapse of the eruptive column. The collapse during pulse I generated the first gravity-driven pyroclastic surge over the lava flow field and lasted ~10 s, as estimated from seismic and acoustic signals. The corresponding deposit (unit I) formed by both unaltered and hydrothermally altered, cold material, matches well the dark color (temperature lower than 100°C) of the pyroclastic density current recorded by the INGV thermal camera [*Calvari et al.*, 2010]. Within this eruptive phase, a large number of hot blocks were ejected with an estimated initial velocity of 100–155 m/s, which is one order of magnitude higher respect to normal Strombolian activity [*Chouet et al.*, 1974; *Patrick et al.*, 2007; *Ripepe et al.*, 1993].

[56] Deposition of unit I over the lava field was completed before the deposition of pyroclasts ejected during pulse II. This was marked by the formation of a convective plume that drifted to the west, carried by local winds. The eruptive plume caused tephra fallout with a total volume of 1.7–2 × 10^4 m^3 around the crater area and down into the village of Ginostra. During pulse II, a subsidiary surge was also emplaced on the lava field. Considering 12 s as the duration of the sustained phase of pulse II, we have estimated an average mass discharge rate (MDR) of 1.9–2.3 × 10^6 kg/s.

[57] A final phase of intense but relatively low-pressure degassing from the crater area was recorded by the thermal camera and the infrasonic monitoring station. This phase (pulse III) started at 20:41:33 UT and lasted for 30 s. This was also visible in the thermal camera and likely produced the emplacement of the final scoria flow on the lava flow field (unit III). The deposit, with an estimated volume of 1.5–1.7 × 10^4 m^3, is observed to seal the pulse II tephra, and, considering a total duration of 30 s and a deposit density of 1200 kg/m^3, it corresponds to a mass discharge rate of 5.9–6.7 × 10^5 kg/s.

9. Comparison With Historical Paroxysms

[58] Paroxysms that occurred at the Stromboli volcano in the last two centuries have been described in several scientific papers in terms of ejected materials and their impact on

Table 1. Comparison of the Main Physical Parameters of 5 April 2003 and 15 March 2007 Paroxysms[a]

Parameters	15 March 2007	Notes	5 April 2003	Notes
Total duration	~5 min[b]		~8 min[c]	
Fallout volume	$1.7–2 \times 10^4$ m^3[b]	$T = T_0 \exp(-k\sqrt{A})$	$2.2–2.4 \times 10^5$ m^3[c]	$T = T_0 \exp(-k\sqrt{A})$
Fallout mass	$2.2–2.7 \times 10^7$ kg[b]	$T = T_0 \exp(-k\sqrt{A})$	$1.1–1.4 \times 10^8$ kg[c]	$T = T_0 \exp(-k\sqrt{A})$
Fallout MDR	$1.9–2.3 \times 10^6$ kg/s[b]	duration = 12 s	$1.0–1.2 \times 10^7$ kg/s[c]	duration = 11 s
Pyr. flow volume	$1.5–1.7 \times 10^4$ m^3[b]	Unit III scoria flow	$0.9–1.1 \times 10^4$ m^3[c]	scoria flow
Pyr. flow MDR	$5.9–6.7 \times 10^5$ kg/s[b]	duration = 30 s	$2.5–3.1 \times 10^5$ kg/s[c]	duration = 42 s
Ballistic ejection velocity	126 m/s[b]	block on ROC	185 m/s[c,d]	block on ROC
Ballistic ejection velocity	100–155 m/s[b]	full range	150–200 m/s[c,d]	full range
Plume density	13.5 ± 3 kg/m^3[b]	$U_{cloud} = U_{ejecta} + \left[\frac{4g\rho_{ejecta}}{3C_D\rho_{cloud}}\right]\sqrt{D}$	6.7 kg/m^3[d]	$U_{cloud} = U_{ejecta} + \left[\frac{4g\rho_{ejecta}}{3C_D\rho_{cloud}}\right]\sqrt{D}$
Gas velocity	130–210 m/s[b]	thermal camera + ballistics	324 m/s[d]	from radiometer log
Overpressure	7.9 ± 0.4 MPa[b]	$P_{gas} = \rho_{gas}RT/m$	3.8 MPa[d]	$P_{gas} = \rho_{gas}RT/m$
Gas mass fraction	0.008[b]	$U_{cloud}^2 = 2\left[\frac{nRT}{m}\ln\left(\frac{P_{cloud}}{P_{atm}}\right) + \frac{1-n}{\rho_{ejecta}}(P_{cloud} - P_{atm})\right]$	0.025[d]	$U_{cloud}^2 = 2\left[\frac{nRT}{m}\ln\left(\frac{P_{cloud}}{P_{atm}}\right) + \frac{1-n}{\rho_{ejecta}}(P_{cloud} - P_{atm})\right]$
Total gas mass	$1.9–2.3 \times 10^5$ kg[b]	$M_{gas} = [n/(1-n)]M_{ejecta}$	2.9×10^6 kg[d]	$M_{gas} = [n/(1-n)]M_{ejecta}$
Total gas volume	$1.3–1.9 \times 10^4$ m^3[b]		5.7×10^5 m^3[d]	
Column height	2980 m[b]	$H = 0.042M_e^{1/4}$	4000 m[c]	$H = 0.042M_e^{1/4}$
Vent radius	4 m[b]	$R = \sqrt{(Q/U\pi)}$	10 m[b]	$R = \sqrt{(Q/U\pi)}$

[a]Main equations used in calculations are reported in the notes and discussed in the text. For the volume calculation, T refers to the thickness, T_0 is the maximum thickness, A is the area, and k is the slope of the exponential fit. For the vent radius calculation, Q refers to the calculated mass flux, R to the cylinder radius, and U to the calculated ejection velocity of the material during the main event.
[b]Data are from this work.
[c]Data are from *Rosi et al.* [2006].
[d]Data are from *Ripepe and Harris* [2008].

settled areas [*Barberi et al.*, 1993; *Capaldi et al.*, 1978; *Rittmann*, 1931; *Rosi et al.*, 2006]. The 1930 event, very likely the most energetic one, is the eruption that produced the highest number of casualties (at least eight) and has been studied in great detail by *Rittmann* [1931], who gathered residents' accounts, made observation of the deposits, and conducted a topographic survey of the crater changes produced by the explosion. More recently, *Capaldi et al.* [1978] and *Barberi et al.* [1993] have compiled a detailed review of all the events for which information is available. They point out that, in addition to the emission of a large amount of blocks and ash, virtually all the historical events have also ejected highly vesicular and unaltered pumice. Over the past 20 years, the petrology, geochemistry, and volatile contents of this so-called golden pumice, ejected only during the strong explosions, have been extensively investigated [*Di Carlo et al.*, 2006; *Francalanci et al.*, 1999, 2005; *Métrich et al.*, 2001, 2010]. These studies have demonstrated that golden pumice results from the sudden rise and explosion of fairly small pockets (10^3–10^4 m^3) of crystal-poor, volatile-rich magma batches from a depth ranging between 7 and 10 km and passing through a region of Stromboli's conduit that is filled by crystal-rich, and relatively degassed magma [*Bertagnini et al.*, 1999; *Métrich et al.*, 2010].

[59] In recent years, the most intense explosions occurred on 5 April 2003 [*Calvari et al.*, 2006; *Pino et al.*, 2011; *Pistolesi et al.*, 2008; *Ripepe and Harris*, 2008; *Rosi et al.*, 2006] and 15 March 2007 [*Andronico et al.*, 2007]. Both events share a number of features, such as the production of tephra fallout from a convective plume, the ejection of golden pumice, and meter-sized ballistic blocks reaching the inhabited areas, constituting a serious hazard for both people and infrastructures. The 2003 and 2007 events are the only ones for which a number of eruptive parameters are determinable. The main eruptive parameters for the two events, obtained following the same methods [*Ripepe and Harris*, 2008; *Rosi et al.*, 2006], are listed for comparison in Table 1. Although the 2007 event shares most of the typical features of paroxysmal explosions, some peculiar aspects should be emphasized. The common features with past paroxysms are the impulsive nature of the eruption sequence, with the formation of a short-lived and sustained column. The first phase is accompanied by the emission of ballistic blocks dispersed along the direction of the dyke along which the vents are located, as already described. These short-lived explosions are characterized by a rapid decompression with gas-ash jet velocities exceeding 200 m/s and the contemporaneous cannon-like ejection of ballistic blocks with diameters up to 2 m at velocities up to 200 m/s. Blocks likely represent the brittle failure of the conduit wall rocks that is due to the rise of the overpressurized magma slug [*Rittmann*, 1931; *Rosi et al.*, 2006; *Pistolesi et al.*, 2008] or of the partially crystallized shallow plumbing system [*Renzulli et al.*, 2009]. The nonsymmetrical distribution of the blocks west-southwest and northeast of the craters suggests that the ejection direction was controlled by the geometry of the shallow dyke that feeds the summit conduits [*Chouet et al.*, 2003].

[60] Paroxysms always form eruptive columns and attendant convective plumes a few kilometers high. Tephra fallout typically overcomes the coastline of the island and is usually dispersed to the southeast by the dominant winds

coming from the northwest [*Brusca et al.*, 2004]. Because of the impulsive eruption dynamics, tephra fallout is not expected to produce a significant hazard for the island. In proximal locations, however, spatter fallout and the formation of up to meter-thick welded deposits could result in a significant threat for humans, which may be present in the summit areas.

[61] The lower elevation of the main effusive vent during the 2007 eruption, that is, 400 m asl in 2007, compared with 550–670 m during 2002–2003, may have caused the higher effusion rates during 2007 [*Calvari et al.*, 2010], and in turn was responsible for the fast drainage of the magmatic column which lead to the summit collapse. We propose that the collapse of the summit area before the paroxysm may have affected the dynamics of the explosion. The particular configuration of the crater area, in fact, may be responsible for the high overpressure of the main explosion, which was double that of the 2003 event (7.9 $\pm$ 0.4 versus 3.8 MPa), despite the lower erupted gas volume (1.3–1.9 $\times$ 10^4 versus 5.7 $\times$ 10^5 m^3). The initial explosion was likely triggered by the arrival of the overpressurized gas slug whose decoupling from the LP magma batch could also have been favored by conduit obstruction and clogging.

[62] The large volume of loose debris resulting from cone collapse was then incorporated into the eruptive mixture. This high density favored subsequent collapse during the first stage of the paroxysm, with the generation of a pyroclastic flow that remained confined within the Sciara del Fuoco (unit I). After the first explosion, the LP magma likely underwent rapid decompression and fragmentation, sustaining the second eruptive pulse. Magmatic fragmentation involved both HP and LP magma and formed the second jet, which fed both a convective plume (the windblown fallout over Ginostra) and the pyroclastic surge of unit II. The last portion of the already degassed LP magma batch was emitted during the final stage. This was unable to generate a convective plume and evolved through a "boiling-over" activity with the formation of a scoria flow onto the Sciara del Fuoco (unit III).

[63] Significant preeruptive degassing and the formation of a decoupled gas slug during the very first stage of the paroxysm is in apparent conflict with the greater vesicularity of the LP pumice fragments emitted at a later stage (pulse 2) with respect to the same tephra products of the 2003 eruption. However, the 2007 pumice shows little evidence of mingling with the gas-poor HP magma. We know from the 2003 event that the mingling has, not surprisingly, a major effect in lowering the vesicularity of pumice clasts. Tephra of the 2007 explosion are characterized by golden pumice with little HP-LP mingling and also by the scarcity of unaltered HP scoria in ejecta. This is a remarkable difference with respect to the 2003 event that was instead characterized by a large quantity of prominently mingled HP-LP clasts.

10. Concluding Remarks

[64] The persistent low-intensity activity of Stromboli has been interrupted during the last 10 years by two eruptive crises in 2002–2003 and in 2007. These two crises were remarkably similar and consisted of lava emission from lateral vents, the temporary cessation of the Strombolian activity, and the occurrence of violent explosions (paroxysms). The more intensive and comprehensive geophysical instruments and fieldwork on targeted sites have provided an accurate assessment of the 15 March 2007 eruptive parameters.

[65] In comparison with the 5 April 2003 eruption, the 2007 event has been characterized by a higher initial gas overpressure. This is a remarkable aspect considering that the total mass of erupted gas was much lower than that in the 5 April 2003 event. The collapse of the summit cone and conduits before the 15 March 2007 eruption [*Marsella et al.*, 2009; *Neri and Lanzafame*, 2009] may have favored the gas-LP melt decoupling, resulting in a doubled overpressure (7.9 $\pm$ 0.4 in 2003 versus 3.8 MPa in 2007) and density of the eruptive mixture (13.5 $\pm$ 3 versus 6.7 kg/m^3), despite the lower erupted gas volume (1.3–1.9 $\times$ 10^4 versus 5.7 $\times$ 10^5 m^3). Efficient decoupling of the gas from the magma is indicated by the lack of LP tephra in the early erupted material.

[66] Comparison with other similar historical events shows that Strombolian paroxysms typically are short-lived events consisting of a violent, climactic initial phase lasting a few hundreds of seconds, followed by a minutes-lasting waning tail. The climactic phase is driven by the efficient fragmentation of a volatile-rich, overpressurized magma body, whose dynamics and peak MDRs are typical of subplinian style eruptions ($\sim$10 $\times$ 10^6 kg/s) [*Cioni et al.*, 2000], but with a total magnitude and duration up to two to three orders smaller. The dynamics also appear distinct from violent Strombolian eruptions, which show a similar pulsatory, unsteady nature, but have a longer duration. On the other hand, the comparison with violent Strombolian activity reveals similar dynamics (repetition of individual pulses) but also a much longer duration (months to years) [*Pioli et al.*, 2008].

[67] The duration and magnitude of Strombolian paroxysms are more typical of the vulcanian style. Gas and pyroclasts are ejected with high velocities, similar to those estimated during vulcanian eruptions, for example, Arenal in 1968 or Ngauruhoe in 1975 [*Fagents and Wilson*, 1993; *Melson*, 1972; *Nairn*, 1976], but they are distinct in terms of fragmentation dynamics. In fact, typical vulcanian eruptions are usually associated with the high-pressure buildup within a very viscous and crystalline intermediate to silicic magma.

[68] For these reasons, the classifications of the Strombolian paroxysms hardly fit in the classical eruption styles, making problematic and debatable the use of current terms. They somehow represent atypical Strombolian events characterized by very efficient fragmentation, production of basaltic "pumice," a fairly high mass discharge rate (high intensity), and moderate total erupted mass (moderate magnitude).

Appendix A: Sources of Error and Their Implications

[69] All parameters presented in this paper (erupted material masses, deposit volumes, ejecta velocities) are affected by different sources of error that are due to instrumental characteristics, processing procedures, and physical assumptions (Table A1).

[70] The fallout volume is, for example, affected by a 10% of error relative to GPS positioning, isopach drawing, and extrapolation to account for the fine ash deposited over the

Table A1. Main Parameters Calculated in This Paper and Associated Errors

Parameters	Source of Error	Measurement Error	Model Uncertainty	Relative Error
Fall-out volume	GPS positioning	±5 m		±10%
	Isopach drawing	± 20 m		
Pyr. flow volume	Thickness	±20%		±13%
Pyr. flow velocity	Back-azimuth timing	±2.5 s		±2%
	Back-azimuth angle	± 0.4° (±2 m at 300 m)		
Ballistic ejection velocity (ROC)	Landing time	±0.01 s		±1%
	Starting position	± 10 m		
Ballistic ejection velocity (other blocks)	Equivalent diameter	±0.1 m		±18%
	Time flight/launch angle	± 25 m/s		
Gas velocity	Fitting of eq. diam. VS ejection velocity		±30 m/s	±20%
	Thermal resolution	0.1°C		
	ROC camera acquisition	± 0.25 s		
	Plume height (camera pixel resolution)	± 1 m		
Plume density	Ballistic velocity		±1%	±20%
	Gas-ash velocity		± 20%	
Overpressure	Gas mainly as H_2O		±5%	±5%
Gas mass fraction	Gas at atmospheric P		±10%	±10%
Total gas mass	Error on mass of deposit		±10%	±10%
Total gas volume	Error on plume density		±20%	±20%

sea. The volume of the pyroclastic flow deposit (unit III) is also affected by an error that derives from mapping uncertainties and the use of the deposit average thickness. Assuming a variability of ±20% of the average deposit thickness, we obtain a final error of 13% for the calculated volume of the pyroclastic flow. Propagation velocity of the same pyroclastic flow is calculated by the shift of the location of the infrasonic source. The back azimuth is processed in a 5 s window that gives an uncertainty of ±2.5 s for the onset of the phenomena, whereas the azimuthal resolution of the method used is ±0.4° [*Ripepe et al.*, 2010], corresponding to a spatial resolution of ±2.3 m at a distance of ~300 m from the source. Thus the final error on pyroclastic flow velocity is of the order of <1 m/s.

[71] Ballistic calculations are related to the instrumental characteristics of the seismic station. As we consider only the timing, and since the data are sampled at 54 Hz, the time resolution of the method used is ±0.01 s, which can be considered largely acceptable. Errors on the ballistic velocity of blocks depend also on the timing of the thermal cameras at ROC and SCI. Thermal images were acquired at 2 and 1 Hz, with a resolution in the time of ±0.25 and ±0.5 s, respectively. The other source of error to be considered when estimating block velocity is related to the unknown launch angles and times of flight. All these uncertainties can lead to a discrepancy for a single block as large as 25 m/s, with a final error of 18% for the estimated block velocity.

[72] Gas velocity has been estimated with two approaches: One is "ballistic" and the other is "thermal." For both methods, the main sources of error are partly related to the characteristics of the instruments used (thermal resolution and/or pixel resolution of the thermal cameras) and partly to the velocities of ballistic blocks. We thus estimate a relative error of the order of 20%.

[73] Plume density, overpressure, and total gas mass values given in this paper can also be affected by errors propagating from the above mentioned source parameters (ballistic and ash cloud velocities) and on the model used (see Table 1); these are of the order of 5%–20%.

[74] However, we point out that the same methodology was applied to derive eruptive parameters from two different paroxysms (5 April 2003 and 15 March 2007), and thus they have similar associated errors. This means that, considering relative uncertainties of 20%, the data presented here can be used to fully compare these two explosions.

[75] **Acknowledgments.** This work was partially funded by the Italian "Dipartimento della Protezione Civile" in the framework of the 2007–2009 Agreement (Project V2 - Paroxysm) with Istituto Nazionale di Geofisica e Vulcanologia, INGV. The volcanological guides of Stromboli and the Guardia di Finanza alpine guides are acknowledged for having provided fundamental support during field activities throughout and after the 2007 eruptive crisis. A. Bertagnini and K. V. Cashman are acknowledged for fruitful discussions and for help during the fieldwork. We are also indebted to T. Ricci for having kindly shared photographic material and GPS data. The work greatly benefited from the careful revision of Associate Editor Michael P. Ryan and of two anonymous reviewers. A. Revil is acknowledged for editorial assistance.

References

Aiuppa, A., C. Federico, G. Giudice, G. Giuffrida, R. Guida, S. Guerrieri, M. Liuzzo, R. Moretti, and P. Papale (2009), The 2007 eruption of Stromboli volcano: Insights from real-time measurement of the volcanic gas plume CO_2/SO_2 ratio, *J. Volcanol. Geotherm. Res.*, *182*(3–4), 221–230, doi:10.1016/j.jvolgeores.2008.09.013.

Andronico, D., A. Cristaldi, and J. Taddeucci (2007), Eruzione Stromboli 2007–L'evento parossistico del 15 marzo, *Int. Rep. UFVG2007/016*, INGV, Sezione di Catania, Italy. (Available at http://193.206.223.22/Report/RPTVSTRCEN20070315.pdf.)

Barberi, F., M. Rosi, and A. Sodi (1993), Volcanic hazard assessment at Stromboli based on review of historical data, *Acta Vulcanol.*, *3*, 173–187.

Barberi, F., L. Civetta, M. Rosi, and R. Scandone (2009), Chronology of the 2007 eruption of Stromboli and the activity of the Scientific Synthesis Group, *J. Volcanol. Geotherm. Res.*, *182*(3–4), 123–130, doi:10.1016/j.jvolgeores.2008.09.019.

Bertagnini, A., M. Coltelli, P. Landi, M. Pompilio, and M. Rosi (1999), Violent explosions yield new insights into dynamics of Stromboli volcano, *Eos Trans. AGU*, *80*(52), 633–636, doi:10.1029/99EO00415.

Bonaccorso, A., S. Calvari, G. Garfì, L. Lodato, and D. Patanè (2003), Dynamics of the December 2002 flank failure and tsunami at Stromboli volcano inferred by volcanological and geophysical observations, *Geophys. Res. Lett.*, *30*(18), 1941, doi:10.1029/2003GL017702.

Brusca, L., S. Inguaggiato, M. Longo, P. Madonia, and R. Maugeri (2004), The 2002–2003 eruption of Stromboli (Italy): Evaluation of the volcanic activity by means of continuous monitoring of soil temperature, CO_2 flux, and meteorological parameters, *Geochem. Geophys. Geosyst.*, *5*, Q12001, doi:10.1029/2004GC000732.

Burton, M. R., T. Caltabiano, F. Murè, G. Salerno, and D. Randazzo (2009), SO_2 flux from Stromboli during the 2007 eruption: results from the FLAME network and traverse measurements, *J. Volcanol. Geotherm. Res.*, *182*(3–4), 214–220, doi:10.1016/j.jvolgeores.2008.11.025.

Calvari, S., L. Spampinato, and L. Lodato (2006), The 5 April vulcanian paroxysmal explosion at Stromboli volcano (Italy) from field observation and thermal data, *J. Volcanol. Geotherm. Res.*, *149*(1–2), 160–175, doi:10.1016/j.jvolgeores.2005.06.006.

Calvari, S., L. Lodato, A. Steffke, A. Cristaldi, A. J. L. Harris, L. Spampinato, and E. Boschi (2010), The 2007 Stromboli eruption: Event chronology and effusion rates using thermal infrared data, *J. Geophys. Res.*, *115*, B04201, doi:10.1029/2009JB006478.

Capaldi, G., et al. (1978), Stromboli and its 1975 eruption, *Bull. Volcanol.*, *41*, 259–285, doi:10.1007/BF02597227.

Carrigan, C. R. (1994), Two-component magma transport and the origin of composite intrusions and lava flows, in *Magmatic Systems*, edited by M. P. Ryan, pp. 319–354, Academic, San Diego, Calif., doi:10.1016/S0074-6142(09)60102-9.

Casagli, N., A. Tibaldi, A. Merri, C. Del Ventisette, T. Apuani, L. Guerri, J. Fortuny-Guasch, and D. Tarchi (2009), Deformation of Stromboli volcano (Italy) during the 2007 eruption revealed by radar interferometry, numerical modelling and structural geological field data, *J. Volcanol. Geotherm. Res.*, *182*(3–4), 182–200, doi:10.1016/j.jvolgeores.2009.01.002.

Chouet, B., N. Hamisevicz, and T. R. McGetchin (1974), Photoballistics of volcanic jet activity at Stromboli, Italy, *J. Geophys. Res.*, *79*(32), 4961–4976, doi:10.1029/JB079i032p04961.

Chouet, B., P. Dawson, T. Ohminato, M. Martini, G. Saccorotti, F. Giudicepietro, G. De Luca, G. Milana, and R. Scarpa (2003), Source mechanisms of explosions at Stromboli Volcano, Italy, determined from moment-tensor inversions of very-long-period data, *J. Geophys. Res.*, *108*(B1), 2019, doi:10.1029/2002JB001919.

Cioni, R., P. Marianelli, R. Santacroce, and A. Sbrana (2000), Plinian and subplinian eruptions, in *Encyclopedia of Volcanoes*, edited by H. Sigurdson et al., pp. 477–494, Academic, San Diego, Calif.

De Fino, M., L. La Volpe, S. Falsaperla, G. Frazzetta, G. Neri, L. Francalanci, M. Rosi, and A. Sbrana (1988), The Stromboli eruption of December 6, 1985–April 25, 1986: Volcanological, petrological and seismological data, *Bull. Mineral. Rend. Soc. Ital. Mineral. Petrol.*, *43*, 1021–1038.

Delle Donne, D., E. Marchetti, M. Ripepe, G. Ulivieri, and G. Lacanna (2006), Monitoring explosive volanic activity using thermal images, Stromboli volcano, Italy, *Eos Trans. AGU*, *87*(52), Fall Meet. Suppl., Abstract V43B-1795.

Di Carlo, I., M. Pichavant, S. Rotolo, and B. Scaillet (2006), Experimental crystallization of a high-K arc basalt: The Golden Pumice, Stromboli Volcano (Italy), *J. Petrol.*, *47*, 1317–1343, doi:10.1093/petrology/egl011.

Fagents, S. A., and L. Wilson (1993), Explosive volcanic eruptions-VII. The ranges of pyroclasts ejected in transient volcanic explosions, *Geophys. J. Int.*, *113*, 359–370, doi:10.1111/j.1365-246X.1993.tb00892.x.

Falsaperla, S., and L. Spampinato (2003), Seismic insight into explosive paroxysms at Stromboli Volcano, *J. Volcanol. Geotherm. Res.*, *125*(1–2), 137–150, doi:10.1016/S0377-0273(03)00093-3.

Folk, R. L., and W. C. Ward (1957), Brazos River bar: A study in the significance of grain size parameters, *J. Sediment. Petrol.*, *27*, 3–26.

Francalanci, L., S. Tommasini, S. Conticelli, and G. R. Davies (1999), Sr isotope evidence for short magma residence time for the 20th century at Stromboli volcano, Italy, *Earth Planet. Sci. Lett.*, *167*, 61–69, doi:10.1016/S0012-821X(99)00013-8.

Francalanci, L., G. R. Davies, W. Lustenmhower, S. Tommasini, P. R. D. Mason, and S. Conticelli (2005), Old crystal re-cycle and multiple magma reservoirs in the plumbing system of the present day activity at Stromboli volcano, South Italy: Sr-isotope in situ microanalyses, *J. Petrol.*, *46*, 1997–2021, doi:10.1093/petrology/egi045.

Freundt, A., and S. R. Tait (1986), The entrainment of high-viscosity magma into low-viscosity magma in eruption conduits, *Bull. Volcanol.*, *48*, 325–339, doi:10.1007/BF01074464.

Hooper, D. M., and G. S. Mattioli (2001), Kinematic Modeling of pyroclastic flows produced by gravitational dome collapse at Soufriere Hills volcano, Montserrat, *Nat. Hazards*, *23*, 65–86, doi:10.1023/A:1008130605558.

Inman, D. L. (1952), Measures for describing the size distribution of sediments, *J. Sediment. Petrol.*, *22*, 125–145.

Landi, P., L. Francalanci, M. Pompilio, M. Rosi, R. A. Corsaro, C. M. Petrone, I. Nardini, and L. Miraglia (2006), The December 2002–July 2003 effusive event at Stromboli volcano, Italy: An insight into the shallow plumbing system by petrochemical studies, *J. Volcanol. Geotherm. Res.*, *155*(3–4), 263–284, doi:10.1016/j.jvolgeores.2006.03.032.

Marchetti, E., R. Genco, and M. Ripepe (2009), Ground deformation and seismicity related to the propagation and drainage of the dyke feeding system during the 2007 effusive eruption at Stromboli volcano (Italy), *J. Volcanol. Geotherm. Res.*, *182*(3–4), 155–161, doi:10.1016/j.jvolgeores.2008.11.016.

Marsella, M., C. Proietti, A. Sonnessa, M. Coltelli, P. Tommasi, and E. Bernardo (2009), The evolution of the Sciara del Fuoco subaerial slope during the 2007 Stromboli eruption: Relation between deformation processes and effusive activity, *J. Volcanol. Geotherm. Res.*, *182*(3–4), 201–213, doi:10.1016/j.jvolgeores.2009.02.002.

Martini, M., et al. (2007), Seismological monitoring of the February 2007 effusive eruption of the Stromboli volcano, *Ann. Geophys.*, *50*(6), 775–788.

Mastin, L. G. (2001), A simple calculator of ballistic trajectories for blocks ejected during volcanic eruptions, *U.S. Geol. Surv. Open File Rep.*, *01-45*.

Melson, W. G. (1972), *Arenal Volcano, Costa Rica: Catastrophic Eruption of 1986–70 and Pre-eruption History, Contr. to Earth Sci.*, Smithsonian Inst. Press, Washington, D. C.

Métrich, N., A. Bertagnini, P. Landi, and M. Rosi (2001), Crystallization driven by decompression and water loss at Stromboli volcano (Aeolian Islands, Italy), *J. Petrol.*, *42*, 1471–1490, doi:10.1093/petrology/42.8.1471.

Métrich, N., A. Bertagnini, and A. Di Muro (2010), Conditions of magma storage, degassing and ascent at Stromboli: new insights into the volcano plumbing system with inferences on the eruptive dynamics, *J. Petrol.*, *51*(3), 603–626, doi:10.1093/petrology/egp083.

Nairn, I. A. (1976), Atmospheric shock waves and condensation clouds from Ngauruhoe explosive eruptions, *Nature*, *259*, 190–192, doi:10.1038/259190a0.

Neri, M., and G. Lanzafame (2009), Structural features of the 2007 Stromboli eruption, *J. Volcanol. Geotherm. Res.*, *182*(3–4), 137–144, doi:10.1016/j.jvolgeores.2008.07.021.

Parfitt, E. A., and L. Wilson (2008), *Fundamentals of Physical Volcanology*, Blackwell, Cambridge, Mass.

Patrick, M. R., A. J. L. Harris, M. Ripepe, J. Dehn, D. A. Rothary, and S. Calvari (2007), Strombolian explosive styles and source conditions: Insights from thermal (FLIR) video, *Bull. Volcanol.*, *69*, 769–784, doi:10.1007/s00445-006-0107-0.

Pino, N. A., M. Ripepe, and G. B. Cimini (2004), The Stromboli Volcano landslides of December 2002: A seismological description, *Geophys. Res. Lett.*, *31*, L02605, doi:10.1029/2003GL018385.

Pino, N. A., R. Moretti, P. Allard, and E. Boschi (2011), Seismic precursors of a basaltic paroxysmal explosion track deep gas accumulation and slug upraise, *J. Geophys. Res.*, *116*, B02312, doi:10.1029/2009JB000826.

Pioli, L., E. Erlund, E. Johnson, K. V. Cashman, P. Wallace, M. Rosi, and H. Delgado Granados (2008), Explosive dynamics of violent strombolian eruptions: The eruption of Parícutin volcano 1943–1952 (Mexico), *Earth Planet. Sci. Lett.*, *271*, 359–368, doi:10.1016/j.epsl.2008.04.026.

Pistolesi, M., M. Rosi, L. Pioli, A. Renzulli, A. Bertagnini, and D. Andronico (2008), The paroxysmal explosion and its deposits, in *The Stromboli Volcano: An Integrated Study of the 2002–2003 Eruption*, *Geophys. Monogr. Ser.*, vol. 182, edited by S. Calvari et al., pp. 317–329, AGU, Washington, D. C., doi:10.1029/182GM26.

Pompilio, M., and M. Coltelli (1997), Gaining a new insight into the dynamics of the shallow magmatic reservoir of Stromboli volcano from the study of pyroclasts features, paper presented at Volcanic Activity and the Environment, IAVCEI General Assembly, Puerto Vallarta, Mexico.

Pyle, D. M. (1989), The thickness, volume and grain size of tephra fall deposits, *Bull. Volcanol.*, *51*, 1–15.

Renzulli, A., S. Del Moro, M. Menna, P. Landi, and M. Piermattei (2009), Transient processes in Stromboli's shallow basaltic system inferred from dolerite and magmatic breccia blocks erupted during the 5 April 2003 paroxysm, *Bull. Volcanol.*, *71*, 795–813, doi:10.1007/s00445-009-0265-y.

Ripepe, M., and A. J. L. Harris (2008), Dynamics of the 5 April 2003 explosive paroxysm observed at Stromboli by a near-vent thermal, seismic and infrasonic array, *Geophys. Res. Lett.*, *35*, L07306, doi:10.1029/2007GL032533.

Ripepe, M., and E. Marchetti (2002), Array tracking of infrasonic sources at Stromboli volcano, *Geophys. Res. Lett.*, *29*(22), 2076, doi:10.1029/2002GL015452.

Ripepe, M., M. Rossi, and G. Saccorotti (1993), Image processing of the explosive activity at Stromboli, *J. Volcanol. Geotherm. Res.*, *54*(3–4), 335–351, doi:10.1016/0377-0273(93)90071-X.

Ripepe, M., S. Ciliberto, and M. Della Schiava (2001), Time constraints for modeling source dynamics of volcanic explosions at Stromboli, *J. Geophys. Res.*, *106*, 8713–8727, doi:10.1029/2000JB900374.

Ripepe, M., D. Delle Donne, G. Lacanna, E. Marchetti, and G. Ulivieri (2009), The onset of the 2007 Stromboli effusive eruption recorded by an integrated geophysical network, *J. Volcanol. Geotherm. Res.*, *182*(3–4), 131–136, doi:10.1016/j.jvolgeores.2009.02.011.

Ripepe, M., S. De Angelis, G. Lacanna, and B. Voight (2010), Observation of infrasonic and gravity waves at Soufrière Hills Volcano, Montserrat, *Geophys. Res. Lett.*, *37*, L00E14, doi:10.1029/2010GL042557.

Rittmann, A. (1931), Der Ausbruch des Stromboli am 11 September 1930, *Z. Vulkanol.*, *14*, 47–77.

Rosi, M., A. Bertagnini, and P. Landi (2000), Onset of the persistent activity at Stromboli volcano, *Bull. Volcanol.*, *62*, 294–300, doi:10.1007/s004450000098.

Rosi, M., A. Bertagnini, A. J. L. Harris, L. Pioli, M. Pistolesi, and M. Ripepe (2006), A case history of paroxysmal explosion at Stromboli: Timing and dynamics of the April 5, 2003 event, *Earth Planet. Sci. Lett.*, *243*, 594–606, doi:10.1016/j.epsl.2006.01.035.

Self, S., L. Wilson, and I. A. Nairn (1979), Vulcanian eruption mechanisms, *Nature*, *277*, 440, doi:10.1038/277440a0.

Spinetti, C., M. F. Buongiorno, F. Doumaz, M. Musacchio, V. Lombardo, A. J. L. Harris, A. Steffke, and S. Amici (2007), Rapporto eruzione Stromboli 9–16 Marzo 2007, INGV sezione CNT- LABTEL and Univ. of Hawaii - HIGP/SOEST. (Available at http://193.206.223.22/Report/BollettinoCNT_160307_Stromboli%20%282%29.pdf.)

Steinberg, G. S., and J. L. Babenko (1978), Gas velocity and density determination by filming gas discharges, *J. Volcanol. Geotherm. Res.*, *3*(1–2), 89–98, doi:10.1016/0377-0273(78)90005-7.

Tibaldi, A., C. Corazzato, T. Apuani, and A. Cancelli (2003), Deformation at Stromboli volcano (Italy) revealed by rock mechanics and structural geology, *Tectonophysics*, *361*, 187–204, doi:10.1016/S0040-1951(02)00589-9.

Yamasato, H. (1997), Quantitative analysis of pyroclastic flows using infrasonic and seismic data at Unzen volcano, Japan, *J. Phys. Earth*, *45*, 397–416, doi:10.4294/jpe1952.45.397.

D. Delle Donne and M. Ripepe, Dipartimento di Scienze della Terra, Università di Firenze, v. La Pira 4, I-50121 Florence, Italy.

L. Pioli, Section des Sciences de la Terre et de l'Environnement, Université de Genève, rue des Maraîchers 13, CH-1205 Genève, Switzerland.

M. Pistolesi and M. Rosi, Dipartimento di Scienze della Terra, Università di Pisa, v. Santa Maria 53, I-56126 Pisa, Italy. (pistolesi@dst.unipi.it)